ACS OMEGA

http://pubs.acs.org/journal/acsodf

Article

Semitransparent Solar Cells Employing n-Type Graphene on $LaVO_3$

Dong Hee Shin,[§] Dae Ho Jung,[§] and Hosun Lee*

Cite This: *ACS Omega* 2023, 8, 18695−18701

Read Online

ACCESS | Metrics & More | Article Recommendations | Supporting Information

ABSTRACT: To effectively utilize solar energy, semitransparent solar cells are essential in various fields such as building-integrated solar power generation and portable solar chargers. We report triethylenetetramine (TETA)-doped graphene (Gr) transparent conductive electrode (TCE)-based $LaVO_3$ semitransparent solar cells. To optimize the Gr TCE, we varied the TETA molar concentration (n_D) from 0.1 to 0.3 mM. TETA-doped Gr (TETA-Gr)/$LaVO_3$ semitransparent solar cells exhibit the highest 1.45% efficiency and 62% average visible transmittance at n_D = 0.2 mM. These results indicate that the TETA-Gr/$LaVO_3$ structure not only harvests solar energy in the ultraviolet−visible region but also exhibits translucency, thanks to the thin film. Thanks to its translucent properties, we improved the power conversion efficiency (PCE) to 1.99% by adding an Al reflective mirror to the semitransparent cells. Finally, the device's PCE loss is only within 3% for 3000 h in air, suggesting good durability.

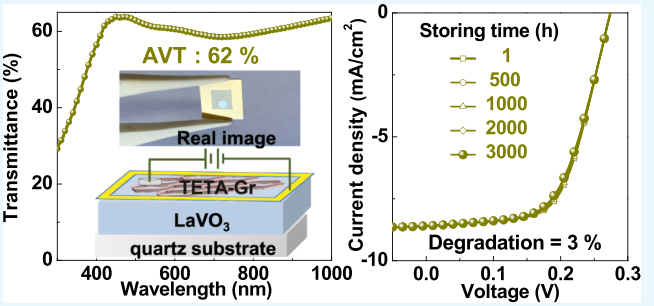

1. INTRODUCTION

Concentrated interest in renewable energy is growing due to alarming climate change around the world.[1] Among new and renewable energy, a solar cell with a safe energy supply form is a device that directly converts electricity using solar energy.[2] To continue the growth of solar energy, obstacles need to be addressed, that is, the low energy density of solar lighting. One way to increase energy density is to integrate semitransparent photovoltaic modules into skyscrapers, unwanted transparent surfaces in automobiles, and window panels in private homes. Currently, organic and perovskite materials are attracting attention as candidates for semitransparent solar cells, and anodes/cathodes used in semitransparent solar cells are generally transparent conductive oxides (TCOs) and metal electrodes.[3−10] However, both the TCO and metal electrodes are disadvantageous in terms of light transmittance (T), making them unsuitable for semitransparent solar cell applications. In addition, organic and perovskite solar cells have excellent efficiency, but their low durability limits their commercialization.[11−15]

On the other hand, graphene (Gr) with perfect light T, high carrier mobility, thermal stability, and excellent conductivity has recently been spotlighted as a next-generation transparent conductive electrode (TCE).[16−18] If Gr TCE is used in semitransparent solar cells, the aperture ratio can be increased while being visually transparent. Although pristine-Gr shows excellent T in the 300−1000 nm region compared to conventional TCO, it has limitations in high-performance semitransparent solar cells due to its low conductivity. For high-performance semitransparent solar cells, a method to improve the conductivity while maintaining excellent T of Gr is required. Chemical doping is one of the techniques to reduce the sheet resistance (R_s) of Gr simply,[19−23] but the R_s of Gr increases over time due to deterioration in air. Therefore, it is very important to find a dopant that can maintain the R_s of Gr for a long time at room temperature. In a previous report,[21−23] we demonstrated high T and long-term stability in the atmosphere for triethylenetetramine (TETA)-doped Gr (TETA-Gr). In addition, the TETA-Gr-based solar cell device demonstrated high stability.[23]

Among the perovskite oxides, $LaVO_3$ can be fabricated as a thin film because of its high absorption coefficient.[25−28] In addition, it is advantageous from an economic point of view because the supply and demand conditions are excellent. Considering these conditions, the $LaVO_3$ film is suitable for use as a practical semitransparent solar cell with long-term stability. Here, we successfully demonstrate a TETA-Gr/$LaVO_3$ heterojunction solar cell as a function of doping concentrations (n_D). The power conversion efficiency (PCE) of the device is maximized to be 1.45% at n_D = 0.2 mM due to the R_s and T correlation of TETA-Gr and the ideality factor (n) and decay/rise time ratio in the device. Besides, the device's average visible T (AVT) is 62% translucent. To improve the performance of the translucent TETA-Gr/$LaVO_3$ solar cell, we use an Al mirror to increase the unit current

Received: January 29, 2023
Accepted: May 4, 2023
Published: May 15, 2023

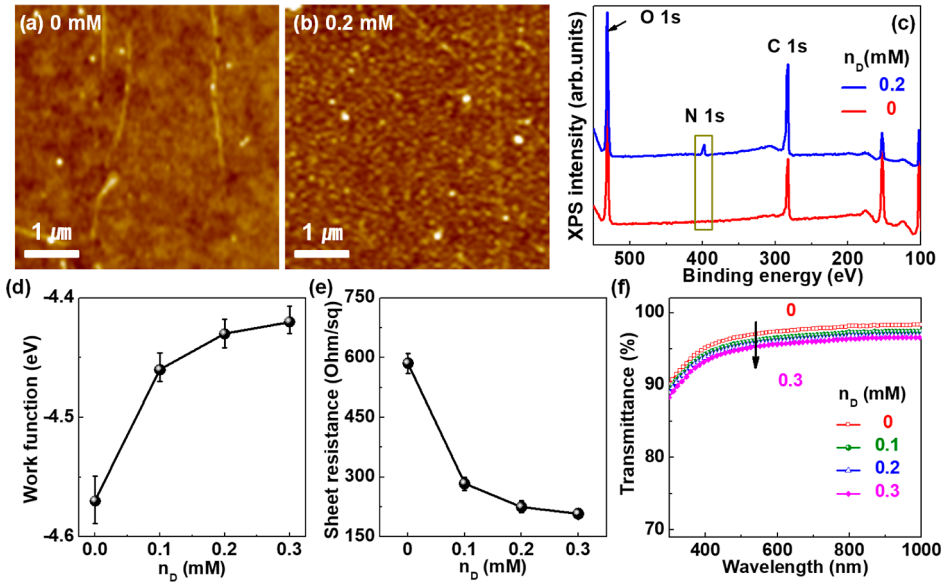

Figure 1. AFM topographical images of TETA-Gr for n_D = (a) 0 and (b) 0.2 mM and (c) XPS spectra of TETA-Gr for n_D = 0 and 0.2 mM. (d) Work functions, (e) sheet resistance, and (f) transmittance of single-layer Gr TCEs doped by TETA with different concentrations (n_D) of 0, 0.1, 0.2, and 0.3 mM.

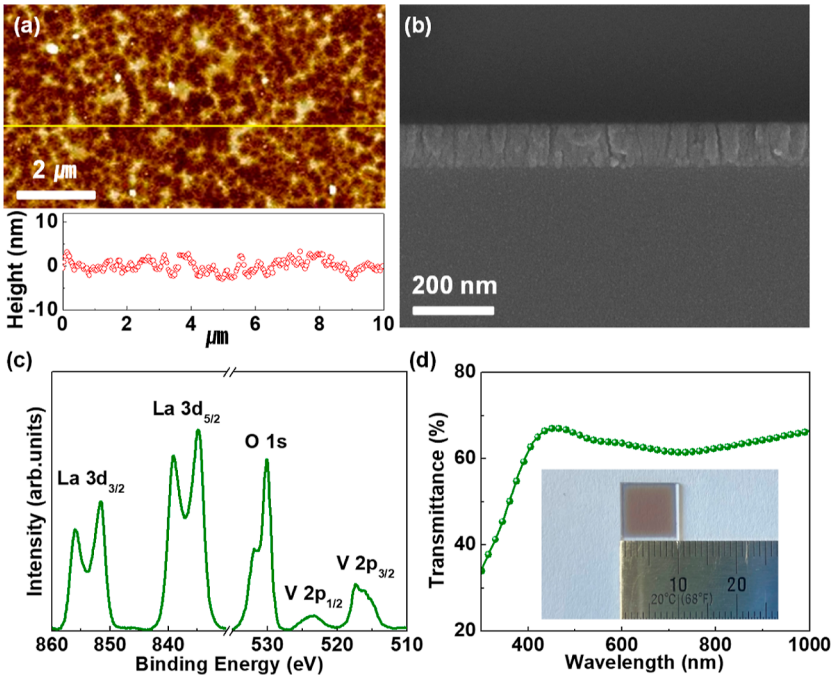

Figure 2. (a) AFM morphological images, (b) cross-sectional SEM image, (c) XPS spectrum, and (d) transmittance spectrum/real image of $LaVO_3$ film.

density by about 33%, improving the PCE to 1.99%. Finally, the device's PCE retains 97% of its original PCE even after 3000 h in an atmosphere with 25 °C temperature and 35−40% relative humidity.

2. EXPERIMENTAL SECTION

2.1. Fabrication of TETA-Doped Graphene/$LaVO_3$ Semitransparent Solar Cells. To synthesize the $LaVO_3$ film on the quartz substrate, we deposited them using a radio frequency magnetron sputtering system under a H_2 (35%)/Ar mixture gas atmosphere for 4 h. Single-layer Gr on a Cu foil substrate was grown while injecting CH_4 and H_2 gases in a chemical vapor deposition (CVD) furnace at 1000 °C. Sequentially, it was transferred onto a $LaVO_3$ substrate through a well-known wet process. To prepare molar concentration (n_D)-dependent TETA solutions, we dissolved different amounts of TETA molecules in ethanol. We prepared n_D between 0 and 0.3 mM. To adsorb TETA molecules on the pristine-Gr surface, they were spin-coated at 3000 rpm for 1 min and immediately annealed at 70 °C for 30 min. To complete the semitransparent device, we deposited Ag and Au films as the top and bottom electrodes, respectively. We fixed the active area of the device to 25 mm^2.

https://doi.org/10.1021/acsomega.3c00598
ACS Omega 2023, 8, 18695−18701

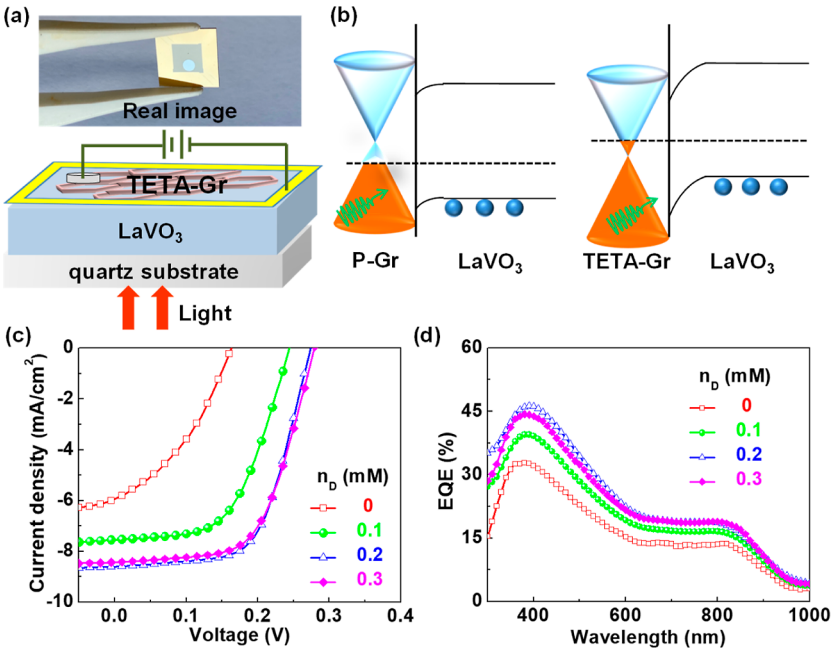

Figure 3. (a) Schematic/real image of the TETA-Gr/$LaVO_3$ device/and (b) energy band diagram of a typical pristine-Gr(P-Gr)/$LaVO_3$ and TETA-Gr/$LaVO_3$ solar cell. (c) Typical $J-V$ curves and (d) EQE spectra of solar cells under 1 sun illumination (100 mW/cm^2, air mass 1.5 global) as a function of n_D.

2.2. Characterizations. To acquire the topographical images of bare- and TETA-Gr, we used a non-contact atomic force microscope (Park System model XE-100). To check the atomic bonding state of TETA-Gr, we measured and analyzed the X-ray photoelectron spectroscopy (XPS) spectrum by the Al kα line with 1486.6 eV. Ultraviolet (UV)−visible T/absorbance spectra covering the 300−1000 nm wavelength range were measured by a Varian Cary-5000 spectrophotometer. To measure the R_s and work function for TETA-Gr TCE, we measured 4-probe method (Dasol-eng model FPP-HS8-40K) and Kelvin-probe force microscope (Park System model XE-100). To complete the solar cell, we deposited Ag and Au on the front and rear electrodes, respectively, considering the work functions of TETA-Gr and $LaVO_3$ materials. To measure the photovoltaic parameters of the TETA-Gr/$LaVO_3$ device, we investigated the current density−voltage ($J-V$) behavior under a solar simulator (McScience model K201) with 1 sun (100 mW/cm^2, air mas 1.5 global). The device's external quantum efficiency (EQE) was measured by using a Newport 74125 instrument.

3. RESULTS AND DISCUSSION

An atomic force microscopy (AFM) image in Figure 1a,b shows the surface morphology of TETA-Gr sheets for n_D = 0 and 0.2 mM. Figure 1c shows the XPS spectra of C 1s, N 1s, and O 1s core levels for TETA-Gr sheets at n_D = 0 and 0.2 mM. As expected, the N 1s peak exists only on the TETA-Gr surface, thereby suggesting successful doping of the TETA. Figure 1d shows the work function of TETA-Gr as a function of n_D. The work function of pristine-Gr is −4.57 eV and decreases monotonically to −4.41 eV as n_D increases to 0.3 mM, demonstrating n-type doping.[23] Electron-donating aromatic molecules such as −amine (−NH_2) and −dimethyl (−CH_3) bind stably to Gr to form n-type Gr.[21−23] The R_s decreases monotonically from ∼590 to 208 Ω/sq as n_D increases up to 0.3 mM (Figure 1e), consistent with the previous literature.[23] Figure 1f shows the T of TETA-Gr for different n_D. Unlike metal particles, the T of Gr doped with TETA is almost constant regardless of n_D.[23,24] To confirm the potential of TETA-Gr as a practical TCE, a composite manner analysis of R_s and T is required. In general, the performance of a TCE is evaluated by calculating the ratio of DC conductivity/photoconductivity (σ_{DC}/σ_{op}) by the following equation $T = \{1 + (Z_0/2R_s)(\sigma_{op}/\sigma_{DC})\}^{-2}$,[29] where Z_0 is the impedance of free space. High T and low R_s indicate high σ_{DC}/σ_{op}, which means good TCE. Figure 1f shows the calculated σ_{DC}/σ_{op} values for TETA-Gr as a function of n_D, reaching a maximum of ∼38 at n_D = 0.2 mM.

Figure 2a presents a cross-sectional image of $LaVO_3$ measured by a scanning electron microscopy (SEM) instrument. Figure 2b shows an AFM image of the surface morphology of the $LaVO_3$ film. From the AFM images, the surface roughness (R_q) was measured to be 0.95 nm. Figure 2c shows the XPS binding energy spectrum of the $LaVO_3$ film. Here, the spin−orbit splitting difference between La 3d and V 2p central peaks means that the La/V atomic ratio is close to 1, suggesting that the $LaVO_3$ film is well formed. Figure 2d shows the T of the $LaVO_3$/quartz for wavelengths from 300 to 1000 nm. The T of $LaVO_3$ is >60% in the visible light region, and the AVT is 64%. These results suggest that $LaVO_3$ is a suitable active layer material for semitransparent optoelectronic devices.

Figure 3a shows a schematic diagram of a heterojunction solar cell composed of TETA-Gr TCE and light-absorbing material $LaVO_3$. The energy band diagram of a typical TETA-Gr/$LaVO_3$ solar cell is shown in Figure 3b. Here, the Fermi level and band gap of $LaVO_3$ are quoted from the previous literature. Figure 3c shows the photovoltaic properties of TETA-Gr/$LaVO_3$ solar cells with different n_D under simulated 1 sun illumination (100 mW/cm^2). The pristine-Gr/$LaVO_3$ device displays 0.165 V open-circuit voltage (V_{oc}), 5.95 mA/cm^2, short-circuit current density (J_{sc}), 36.46% fill factor (FF),

https://doi.org/10.1021/acsomega.3c00598
ACS Omega 2023, 8, 18695−18701

Table 1. Photovoltaic Parameters of TETA-Graphene/$LaVO_3$ Solar Cells for Various n_D

n_D (mM)	V_{oc} (V)	J_{sc} (mA/cm^2)	integrated J_{sc} (mA/cm^2)	FF (%)	best PCE (%)	average PCE (%)
0	0.165	5.95	5.65	36.46	0.36	0.32 ± 0.04
0.1	0.240	7.58	7.17	56.25	1.02	0.88 ± 0.14
0.2	0.275	8.60	8.27	61.18	1.45	1.29 ± 0.16
0.3	0.280	8.43	7.98	59.69	1.41	1.26 ± 0.15

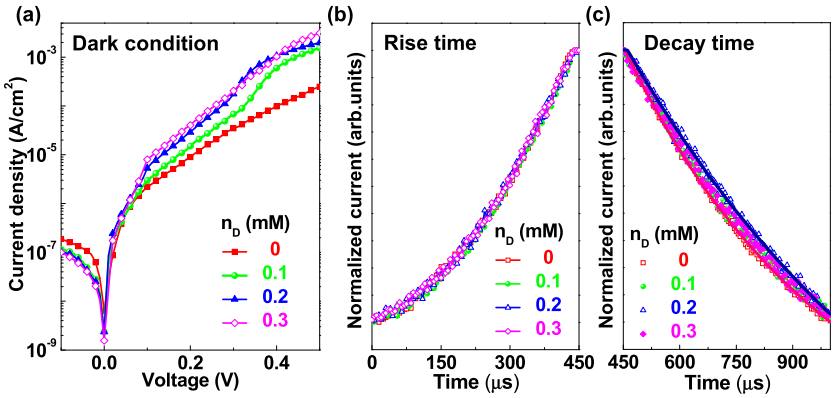

Figure 4. (a) Dark $I-V$ curves and (b,c) normalized transient PCs of TETA-Gr/$LaVO_3$ solar cells for various L_n. The measurements were carried out at $V = 0$ under pulsed-laser excitation at 532 nm.

and 0.36% PCE. Best solar cell performance 0.275 V V_{oc} 8.60 mA/cm^2 J_{sc}, 61.18% FF, and 1.45% PCE was obtained by TETA doping at n_D = 0.2 mM. On the other hand, PCE reaches saturation at n_D > 0.2 mM. The photovoltaic parameters are summarized as a function of the corresponding n_D in Table 1. The highest average PCE for 10 cells as a function of n_D was obtained as 1.29 ± 0.16% at n_D = 0.2 mM (Figure S1).

In all TETA-Gr/$LaVO_3$ solar cells, PCE increases with significantly improved V_{oc} and FF compared to pristine Gr-based devices. These results can be explained by the following reasons: first, n-type doping by TETA increases the Fermi level of Gr by acting as an electron donor. The height of the corresponding Schottky barrier in the TETA-Gr/$LaVO_3$ cells is found to be increased compared to the pristine Gr-based device (Figure 3b).[30] This explains the systematic increase in V_{oc} with increasing n_D. Nevertheless, the reason for the small V_{oc} is that the leakage current increases due to the formation of a small built-in potential in the TETA-Gr/$LaVO_3$ junction, resulting in a small V_{oc}. Second, the improved FF of the device under illumination is mainly due to the reduced R_s with the increased carrier concentration of Gr.

Figure 3d exhibits the EQE spectra from 300 to 1000 nm as a function of n_D. EQE is calculated from the photo harvesting efficiency, charge injection/transfer efficiency, and charge collection efficiency.[31,32] As shown in the EQE spectrum, the EQE gradually increases up to 0.2 mM but decreases slightly at n_D > 0.2 mM. These characteristics are consistent with J_{sc}, as summarized in Table 1, thanks to the close relationship between J_{sc} and integrated values of EQE.[31,32]

We also evaluated the n from the dark $J-V$ behaviors, as shown in Figure 4a. Here, n was calculated by the thermal ion emission theory formula: $J = J_s [\exp(eV/nkT) - 1]$,[33,34] where J_s is the ideal reverse saturation current density. As a result, the n values were 2.85, 2.44, 2.12, and 2.26 at n_D = 0, 0.1, 0.2, and 0.3 mM, respectively. A small n means less probability of recombination at the interface. These results explain why the largest PCE at n_D = 0.2 mM. Figure 4b displays the transient photocurrent (PC) of the device as a function of n_D. The rise/decay times were found to be 268/547, 286/634, 292/892, and 295 μs/835 μs for n_D = 0, 0.1, 0.2, and 0.3 mM, respectively (Table 2). Here, the rise/decay times of each device were

Table 2. Rise/Decay Times and Gain of the TETA-Graphene/$LaVO_3$ Solar Cells as a Function of n_D

n_D (mM)	τ_{rise} (μs)	τ_{decay} (μs)	gain
0	268	547	2.04
0.1	286	634	2.22
0.2	292	892	3.05
0.3	295	835	2.84

calculated through a fitting program. The meaning of rise/decay times is as follows: the time required for the carrier to be generated and then swept with a drift current proportional to the built-in electric field of the cell/the lifetime of the carrier. The gain can be estimated from the ratio of the decay/rise times, thereby estimating the device's carrier collection efficiency. The gains were calculated to be 2.04, 2.22, 3.05, and 2.84 for n_D = 0, 0.1, 0.2, and 0.3 mM, respectively, suggesting that the PC efficiency of the cell can be maximized by controlling n_D. In summary, the results show why the PCE is the largest for TETA-Gr/$LaVO_3$ with n_D = 0.2 mM.

One of the ways to increase the PCE of a semitransparent TFTA-Gr/$LaVO_3$ cell is to improve the efficiency by re-absorbing the transmitted light into the device. Al mirror can reflect light effectively in the UV−visible region (Figure S2).

Figure 5a presents the T spectrum of the TETA-Gr/$LaVO_3$ semitransparent cell at n_D = 0.2 mM. The AVT corresponding to the 400−800 nm range of the cell is 62%, indicating translucency. To improve the efficiency of the device, we measured the photovoltaic parameters using an Al reflection mirror that can effectively reflect light in the UV−visible region. Figure 5b shows a schematic diagram of how a translucent device improves the efficiency by an Al reflection mirror. The measured J_{sc}, V_{oc}, FF, and PCE in the system with

https://doi.org/10.1021/acsomega.3c00598
ACS Omega 2023, 8, 18695−18701

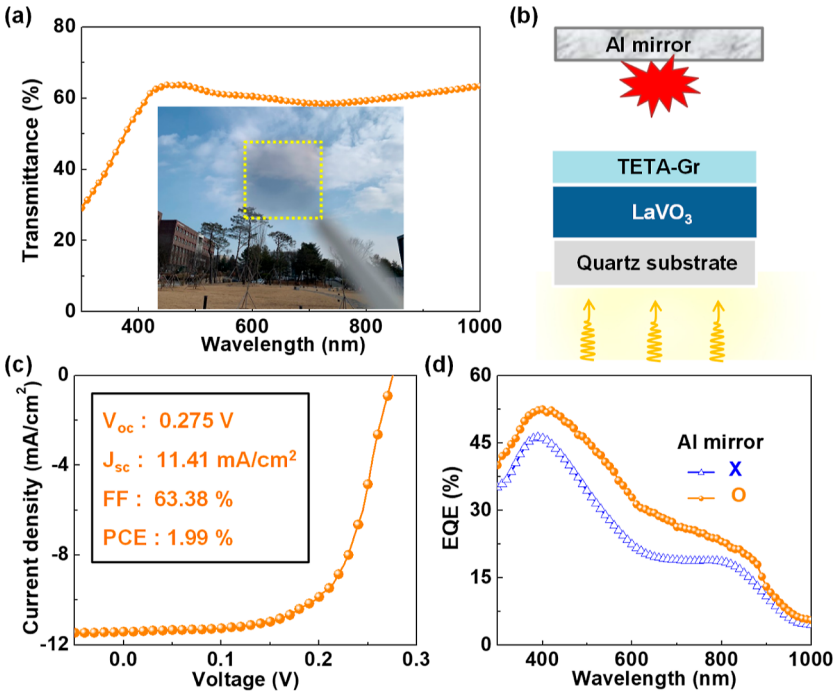

Figure 5. (a) Transmittance spectrum of a typical TETA-Gr/$LaVO_3$ at n_D = 0.2 mM. The inset images show the semitransparent TETA-Gr/$LaVO_3$. (b) Schematic diagram of a semitransparent solar cell with an Al reflective mirror. (c) $J-V$ curves of the semitransparent cell with an Al reflective mirror under illumination from the TETA-Gr side. (d) EQE spectra of devices with/without Al mirror.

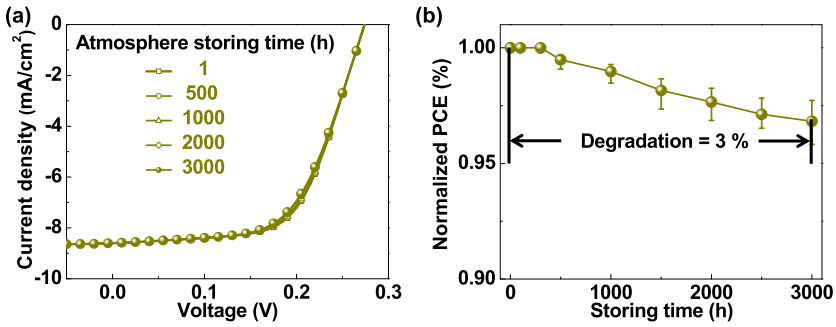

Figure 6. Changes of (a) $J-V$ curve and (b) normalized PCE of the TETA-Gr/$LaVO_3$ solar cell with n_D = 0.2 mM under ambient conditions of 25 °C temperature and 35−40% humidity for 3000 h.

Table 3. Comparison of Maximum PCEs and Their Stabilities of Previously Published Representative Graphene−TCE-Based Semiconductor Solar Cells

device	area (mm^2)	original PCE (%)	degraded PCE (%)	degradation ratio (%)	time (h)	refs
PMMA/TETA-Gr/n-Si	14	5.48	5.37	2.0	700	23
TFSA-Gr/Gr quantum dots/porous Si/n-Si/BCP	9	13.66	12.37	11	700	35
Gr/PEDOT/PSS/Si nanowires/TiO_x	16	3.56	2.39	32	700	36
Ag nanowire-Gr/Si quantum dots/n-Si	16	16.2	13.28	18	700	37
TFSA-Gr/MoS_2/P3HT/PCBM	50	9.60	8.42	10	500	38
Au nanoparticles & TFSA-Gr/Gr quantum dots/$MAPbI_3$/PCBM	16	17.15	12.35	28	700	39
TFSA-Gr/BCP/$MAPbI_3$/Gr quantum dots/$MAPbI_3$/PTAA	16	15.63	14.38	8	500	40
Gr/SAM/GaAs	4	11.1	9.32	16	4000	41
TETA-Gr/$LaVO_3$	25	1.45	1.40	3	3000	this work

Al mirrors are 11.41 mA/cm^2, 0.275 V, 63.38%, and 1.99%, respectively, an approximately 33% increase in PCE compared to the device without Al mirror. J_{sc} obtained from the EQE spectrum of the device with an Al mirror is 10.97 mA/cm^2, demonstrating a significant enhancement of EQE over a wide wavelength range of 400−800 nm compared to the device without Al mirror. These results suggest a significant improvement with the increasing light harvesting efficiency.

To check the device's long-term stability, we monitored the evolution of the PCE for 3000 h (Figure 6). Here, the measurement environment of the device was measured at a temperature of 25 °C and relative humidity of 35−40%. As a

https://doi.org/10.1021/acsomega.3c00598
ACS Omega 2023, 8, 18695−18701

result, the loss of PCE is within 3% of the original PCE (absolutely from 1.45 to 1.40%) during 3000 h (Figure 6b), suggesting higher stability than Gr-based semiconductor solar cells (Table 3).[23,35−41] This result can be explained that the PCE of the TETA-Gr/$LaVO_3$ cell is almost constant because the TETA molecule with a high-molecular weight and a functional group of ethylene amine in bonding to Gr is very stable at air.[42]

4. CONCLUSIONS

We fabricated semitransparent solar cells with n-type Gr TCE and $LaVO_3$ heterojunctions. At n_D = 0.2 mM, the TETA-Gr/$LaVO_3$ device with 25 mm^2 active area achieved 1.45% highest efficiency and 62% AVT. To improve the photovoltaic properties, we increased the maximum PCE to 1.99% by adding an Al mirror to the translucent device. These results demonstrate the realization of stable translucent solar cells owing to $LaVO_3$ thin films and TETA-Gr TCE with high transparency and stability in the air. Furthermore, the device demonstrates remarkable stability, showing comparable levels of the original efficiency even after 3000 h under the atmosphere (25 °C temperature/35−40% relative humidity). This approach proposes a method for fabricating stable translucent optoelectronic devices that can simultaneously achieve the solar efficiency as well as visual effects. It also suggests a very promising new route to develop stable Gr TCE/oxide semiconductor solar cells.

■ ASSOCIATED CONTENT

Supporting Information

The Supporting Information is available free of charge at https://pubs.acs.org/doi/10.1021/acsomega.3c00598.

J−*V* curves of 10 devices for n_D and reflectance spectrum of an Al reflective mirror and real image (PDF)

■ AUTHOR INFORMATION

Corresponding Author

Hosun Lee − *Department of Applied Physics, Institute of Natural Sciences, and Integrated Education Institute for Frontier Science and Technology (BK21 Four), Kyung Hee University, Yongin 17104, Republic of Korea;* orcid.org/0000-0003-0246-4442; Email: hlee@khu.ac.kr

Authors

Dong Hee Shin − *Department of Smart Sensor Engineering, Andong National University, Andong, Gyeongbuk 36729, Republic of Korea*

Dae Ho Jung − *Department of Applied Physics, Institute of Natural Sciences, and Integrated Education Institute for Frontier Science and Technology (BK21 Four), Kyung Hee University, Yongin 17104, Republic of Korea*

Complete contact information is available at: https://pubs.acs.org/10.1021/acsomega.3c00598

Author Contributions

§D.H.S. and D.H.J. contributed equally to this study.

Notes

The authors declare no competing financial interest.

■ ACKNOWLEDGMENTS

This work was supported by the National Research Foundation of Korea (NRF) grant funded by the Ministry of Science, ICT & Future Planning: NRF-2021R1F1A1045446 (H.L.) and NRF-2022R1C1C1008499 (D.H.S.).

■ REFERENCES

(1) Rehbein, J. A.; Watson, J. E. M.; Lane, J. L.; Sonter, L. J.; Venter, O.; Atkinson, S. C.; Allan, J. R. Renewable energy development threatens many globally important biodiversity areas. *Global Change Biol.* **2020**, *26*, 3040−3051.

(2) Li, R.; Shi, Y.; Wu, M.; Hong, S.; Wang, P. Photovoltaic panel cooling by atmospheric water sorption−evaporation cycle. *Nat. Sustainability* **2020**, *3*, 636−643.

(3) Xie, Y.; Cai, Y.; Zhu, L.; Xia, R.; Ye, L.; Feng, X.; Yip, H.-L.; Liu, F.; Lu, G.; Tan, S.; Sun, Y. Fibril Network Strategy Enables High-Performance Semitransparent Organic Solar Cells. *Adv. Funct. Mater.* **2020**, *30*, 2002181.

(4) Wang, D.; Qin, R.; Zhou, G.; Li, X.; Xia, R.; Li, Y.; Zhan, L.; Zhu, H.; Lu, X.; Yip, H.-L.; Chen, H.; Li, C.-Z. High-Performance Semitransparent Organic Solar Cells with Excellent Infrared Reflection and See-Through Functions. *Adv. Mater.* **2020**, *32*, 2001621.

(5) Yin, P.; Yin, Z.; Ma, Y.; Zheng, Q. Improving the charge transport of the ternary blend active layer for efficient semitransparent organic solar cells. *Energy Environ. Sci.* **2020**, *13*, 5177−5185.

(6) Hu, Z.; Wang, J.; Ma, X.; Gao, J.; Xu, C.; Wang, X.; Zhang, X.; Wang, Z.; Zhang, F. Semitransparent organic solar cells exhibiting 13.02% efficiency and 20.2% average visible transmittance. *J. Mater. Chem. A* **2021**, *9*, 6797−6804.

(7) Yu, J. C.; Sun, J.; Chandrasekaran, N.; Dunn, C. J.; Chesman, A. S. R.; Jasieniak, J. J. Semi-transparent perovskite solar cells with a cross-linked hole transport layer. *Nano Energy* **2020**, *71*, 104635.

(8) Li, S.; Wang, C.; Zhao, D.; An, Y.; Zhao, Y.; Zhao, X.; Li, X. Flexible semitransparent perovskite solar cells with gradient energy levels enable efficient tandems with Cu(In,Ga)Se_2. *Nano Energy* **2020**, *78*, 105378.

(9) Gunes, U.; Celik, E. B.; Akgul, C. C.; Koc, M.; Ameri, M.; Uzuner, B. E.; Ghasemi, M.; Sahiner, M. C.; Yildiz, İ.; Kaya, H. Z.; Yerci, S.; Gunbas, G. A Thienothiophene-Based Cation Treatment Allows Semitransparent Perovskite Solar Cells with Improved Efficiency and Stability. *Adv. Funct. Mater.* **2021**, *31*, 2103130.

(10) Yu, Y.; Shang, M.; Wang, T.; Zhou, Q.; Hao, Y.; Pang, Z.; Cui, D.; Lian, G.; Zhang, X.; Han, S. All-round performance improvement of semitransparent perovskite solar cells by a pressure-assisted method. *J. Mater. Chem. C* **2021**, *9*, 15056−15064.

(11) Ghasemi, M.; Balar, N.; Peng, Z.; Hu, H.; Qin, Y.; Kim, T.; Rech, J. J.; Bidwell, M.; Mask, W.; McCulloch, I.; You, W.; Amassian, A.; Risko, C.; O'Connor, B. T.; Ade, H. A molecular interaction−diffusion framework for predicting organic solar cell stability. *Nat. Mater.* **2021**, *20*, 525−532.

(12) Ma, R.; Yan, C.; Yu, J.; Liu, T.; Liu, H.; Li, Y.; Chen, J.; Luo, Z.; Tang, B.; Lu, X.; Li, G.; Yan, H. High-Efficiency Ternary Organic Solar Cells with a Good Figure-of-Merit Enabled by Two Low-Cost Donor Polymers. *ACS Energy Lett.* **2022**, *7*, 2547−2556.

(13) Wang, K.; Li, Y.; Li, Y. Challenges to the Stability of Active Layer Materials in Organic Solar Cells. *Macromol. Rapid Commun.* **2020**, *41*, 1900437.

(14) Niu, T.; Zhu, W.; Zhang, Y.; Xue, Q.; Jiao, X.; Wang, Z.; Xie, Y.-M.; Li, P.; Chen, R.; Huang, F.; Li, Y.; Yip, H.-L.; Cao, Y. D-A-π-A-D-type Dopant-free Hole Transport Material for Low-Cost, Efficient, and Stable Perovskite Solar Cells. *Joule* **2021**, *5*, 249−269.

(15) Cheng, Y.; Ding, L. Pushing commercialization of perovskite solar cells by improving their intrinsic stability. *Energy Environ. Sci.* **2021**, *14*, 3233−3255.

(16) Kim, M.; Nabeya, S.; Han, S.-M.; Kim, M.-S.; Lee, S.; Kim, H.-M.; Cho, S.-Y.; Lee, D.-J.; Kim, S.-H.; Kim, K.-B. Selective Atomic Layer Deposition of Metals on Graphene for Transparent Conducting Electrode Application. *ACS Appl. Mater. Interfaces* **2020**, *12*, 14331−14340.

(17) Hasani, A.; Mohammadzadeh, M. R.; Ghanbari, H.; Fawzy, M.; Silva, T. D.; Abnavi, A.; Ahmadi, R.; Askar, A. M.; Kabir, F.;

Rajapakse, R. K. N. D.; Adachi, M. M. Self-Powered, Broadband Photodetector Based on Two-Dimensional Tellurium-Silicon Heterojunction. *ACS Omega* **2022**, *7*, 48383−48390.
(18) Liudi Mulyo, A.; Mukherjee, A.; Høiaas, I. M.; Ahtapodov, L.; Nilsen, T. A.; Toftevaag, H. H.; Vullum, P. E.; Kishino, K.; Weman, H.; Fimland, B.-O. Graphene-Based Transparent Conducting Substrates for GaN/AlGaN Nanocolumn Flip-Chip Ultraviolet Light-Emitting Diodes. *ACS Appl. Nano Mater.* **2021**, *4*, 9653−9664.
(19) Singh, A. K.; Singh, A. K.; Sinha, S. R. P. Fermi-Level Modulation of Chemical Vapor Deposition-Grown Monolayer Graphene via Nanoparticles to Macromolecular Dopants. *ACS Omega* **2022**, *7*, 744−751.
(20) Zainal Ariffin, N. H.; Mohammad Haniff, M. A. S.; Syono, M. I.; Ambri Mohamed, M.; Hamzah, A. A.; Hashim, A. M. Low-Temperature Nitrogen Doping of Nanocrystalline Graphene Films with Tunable Pyridinic-N and Pyrrolic-N by Cold-Wall Plasma Assisted Chemical Vapor Deposition. *ACS Omega* **2021**, *6*, 23710−23722.
(21) Kim, J. M.; Kim, S.; Choi, S.-H. High-Performance n-i-p-Type Perovskite Photodetectors Employing Graphene-Transparent Conductive Electrodes N-Type Doped with Amine Group Molecules. *ACS Sustainable Chem. Eng.* **2019**, *7*, 734−739.
(22) Shin, D. H.; Jang, C. W.; Lee, H. S.; Seo, S. W.; Choi, S.-H. Semitransparent Flexible Organic Solar Cells Employing Doped Graphene Layers as Anode and Cathode Electrodes. *ACS Appl. Mater. Interfaces* **2018**, *10*, 3596−3601.
(23) Shin, D. H.; Jang, C. W.; Lee, H. S.; Seo, S. W.; Kim, S.; Choi, S.-H. Graphene/Si solar cells employing triethylenetetramine dopant and polymethylmethacrylate antireflection layer. *Appl. Surf. Sci.* **2018**, *433*, 181−187.
(24) Shin, D. H.; Kim, J. M.; Jang, C. W.; Kim, J. H.; Kim, S.; Choi, S.-H. Effect of layer number and metal-chloride dopant on multiple layers of graphene/porous Si solar cells. *J. Appl. Phys.* **2018**, *123*, 123101.
(25) Jung, D. H.; Hwang, J. W.; Lee, J. J.; Shin, D. H.; Lee, H. High-performance and high-stability $LaVO_3$/Si solar cells through employing thickness-controlled $LaVO_3$ and a titanium oxide passivation layer. *J. Alloys Compd.* **2022**, *904*, 163818.
(26) Lee, J. J.; Jung, D. H.; Shin, D. H.; Lee, H. Highly stable semitransparent multilayer graphene/$LaVO_3$ vertical-heterostructure photodetectors. *Nanotechnology* **2022**, *33*, 395202.
(27) Lee, J. J.; Shin, D. H.; Jung, D. H.; Oh, S. D.; Lee, H. A high-performance broadband self-powered photodetector employing an MoS_2/$LaVO_3$ heterojunction structure. *J. Alloys Compd.* **2023**, *937*, 168404.
(28) Lovinger, D. J.; Brahlek, M.; Kissin, P.; Kennes, D. M.; Millis, A. J.; Engel-Herbert, R.; Averitt, R. D. Influence of spin and orbital fluctuations on Mott-Hubbard exciton dynamics in $LaVO_3$ thin films. *Phys. Rev. B* **2020**, *102*, 115143.
(29) De, S.; Coleman, J. N. Are There Fundamental Limitations on the Sheet Resistance and Transmittance of Thin Graphene Films? *ACS Nano* **2010**, *4*, 2713−2720.
(30) Ho, P.-H.; Lee, W.-C.; Liou, Y.-T.; Chiu, Y.-P.; Shih, Y.-S.; Chen, C.-C.; Su, P.-Y.; Li, M.-K.; Chen, H.-L.; Liang, C.-T.; Chen, C.-W. Sunlight-activated graphene-heterostructure transparent cathodes: enabling high-performance n-graphene/p-Si Schottky junction photovoltaics. *Energy Environ. Sci.* **2015**, *8*, 2085−2092.
(31) Jungbluth, A.; Kaienburg, P.; Riede, M. Charge transfer state characterization and voltage losses of organic solar cells. *J. Phys.: Mater.* **2022**, *5*, 024002.
(32) Zhang, C.; Kuang, D.-B.; Wu, W.-Q. A Review of Diverse Halide Perovskite Morphologies for Efficient Optoelectronic Applications. *Small Methods* **2020**, *4*, 1900662.
(33) Shin, D. H.; Kim, S.; Kim, J. M.; Jang, C. W.; Kim, J. H.; Lee, K. W.; Kim, J.; Oh, S. D.; Lee, D. H.; Kang, S. S.; Kim, C. O.; Choi, S.-H.; Kim, K. J. Graphene/Si-Quantum-Dot Heterojunction Diodes Showing High Photosensitivity Compatible with Quantum Confinement Effect. *Adv. Mater.* **2015**, *27*, 2614−2620.
(34) Servaites, J. D.; Ratner, M. A.; Marks, T. J. Organic solar cells: A new look at traditional models. *Energy Environ. Sci.* **2011**, *4*, 4410−4422.
(35) Jang, C. W.; Shin, D. H.; Choi, S.-H. Porous silicon solar cells with 13.66% efficiency achieved by employing graphene-quantum-dots interfacial layer, doped-graphene electrode, and bathocuproine back-surface passivation layer. *J. Alloys Compd.* **2021**, *877*, 160311.
(36) Shin, D. H.; Kim, J. H.; Choi, S.-H. High-Performance Conducting Polymer/Si Nanowires Hybrid Solar Cells Using Multilayer-Graphene Transparent Conductive Electrode and Back Surface Passivation Layer. *ACS Sustainable Chem. Eng.* **2018**, *6*, 12446−12452.
(37) Kim, J. M.; Kim, S.; Shin, D. H.; Seo, S. W.; Lee, H. S.; Kim, J. H.; Jang, C. W.; Kang, S. S.; Choi, S.-H.; Kwak, G. Y.; Kim, K. J.; Lee, H.; Lee, H. Si-quantum-dot heterojunction solar cells with 16.2% efficiency achieved by employing doped-graphene transparent conductive electrodes. *Nano Energy* **2018**, *43*, 124−129.
(38) Shin, D. H.; Jang, C. W.; Ko, J. S.; Choi, S.-H. Enhancement of efficiency and stability in organic solar cells by employing MoS_2 transport layer, graphene electrode, and graphene quantum dots added active layer. *Appl. Surf. Sci.* **2021**, *538*, 148155.
(39) Shin, S. H.; Shin, D. H.; Choi, S.-H. Enhancement of Stability of Inverted Flexible Perovskite Solar Cells by Employing Graphene-Quantum-Dots Hole Transport Layer and Graphene Transparent Electrode Codoped with Gold Nanoparticles and Bis-(trifluoromethanesulfonyl)amide. *ACS Sustainable Chem. Eng.* **2019**, *7*, 13178−13185.
(40) Jang, C. W.; Shin, D. H.; Choi, S.-H. Photostable electron-transport-layer-free flexible graphene quantum dots/perovskite solar cells by employing bathocuproine interlayer. *J. Alloys Compd.* **2021**, *886*, 161355.
(41) Wen, L.; Gao, F.; Yu, Y.; Xu, Z.; Liu, Z.; Gao, P.; Zhang, S.; Li, G. Enhancing the photovoltaic performance of GaAs/graphene Schottky junction solar cells by interfacial modification with self assembled alkyl thiol monolayer. *J. Mater. Chem. A* **2018**, *6*, 17361−17370.
(42) Kim, Y.; Ryu, J.; Park, M.; Kim, E. S.; Yoo, J. M.; Park, J.; Kang, J. H.; Hong, B. H. Vapor-Phase Molecular Doping of Graphene for High-Performance Transparent Electrodes. *ACS Nano* **2014**, *8*, 868−874.

https://doi.org/10.1021/acsomega.3c00598
ACS Omega 2023, 8, 18695−18701